



**HAL**  
open science

# Experimental study of the binding energy of NH<sub>3</sub> on different types of ice and its impact on the snow line of NH<sub>3</sub> and H<sub>2</sub>O

S. Kakkenpara Suresh, F. Dulieu, J. Vitorino, P. Caselli

► **To cite this version:**

S. Kakkenpara Suresh, F. Dulieu, J. Vitorino, P. Caselli. Experimental study of the binding energy of NH<sub>3</sub> on different types of ice and its impact on the snow line of NH<sub>3</sub> and H<sub>2</sub>O. *Astronomy & Astrophysics - A&A*, 2024, 682, 10.1051/0004-6361/202245775 . insu-04822489

**HAL Id: insu-04822489**

**<https://insu.hal.science/insu-04822489v1>**

Submitted on 6 Dec 2024



**HAL** is a multi-disciplinary open access archive for the deposit and dissemination of scientific research documents, whether they are published or not. The documents may come from teaching and research institutions in France or abroad, or from public or private research centers.

L'archive ouverte pluridisciplinaire **HAL**, est destinée au dépôt et à la diffusion de documents scientifiques de niveau recherche, publiés ou non, émanant des établissements d'enseignement et de recherche français ou étrangers, des laboratoires publics ou privés.



Distributed under a Creative Commons Attribution 4.0 International License

# Experimental study of the binding energy of NH<sub>3</sub> on different types of ice and its impact on the snow line of NH<sub>3</sub> and H<sub>2</sub>O

S. Kakkenpara Suresh<sup>1,2</sup>, F. Dulieu<sup>1</sup>, J. Vitorino<sup>1</sup>, and P. Caselli<sup>2</sup>

<sup>1</sup> LERMA, CY Cergy Paris University, 5 mail Gay Lussac, 95000 Neuville-sur-Oise, France

<sup>2</sup> Max Planck Institute for Extraterrestrial Physics, Giessenbachstraße 1, 85748 Garching, Germany  
e-mail: shreyaks@mpe.mpg.de

Received 23 December 2022 / Accepted 27 November 2023

## ABSTRACT

**Context.** Nitrogen-bearing molecules (such as N<sub>2</sub>H<sup>+</sup> and NH<sub>3</sub>) are excellent tracers of high-density and low-temperature regions, such as dense cloud cores. Notably, they could help advance the understanding of snow lines in protoplanetary discs and the chemical evolution of comets. However, much remains unknown about the chemistry of N-bearing molecules on grain surfaces, which could play an important role in their formation and evolution.

**Aims.** In this work, we experimentally study the behaviour of NH<sub>3</sub> on surfaces that mimic grain surfaces under interstellar conditions in the presence of some other major components of interstellar ices (i.e. H<sub>2</sub>O, CO<sub>2</sub>, CO). We measure the binding energy distributions of NH<sub>3</sub> from different H<sub>2</sub>O ice substrates and also investigate how it could affect the NH<sub>3</sub> snow line in protoplanetary discs.

**Methods.** We performed laboratory experiments using the ultra-high vacuum (UHV) set-up VENUS (VErs des NoUvelles Synthèses). We co-deposited NH<sub>3</sub> along with other adsorbates (H<sub>2</sub>O, <sup>13</sup>CO, and CO<sub>2</sub>) and performed temperature programmed desorption (TPD) and temperature programmed-during exposure desorption (TP-DED) experiments. The experiments were monitored using a quadrupole mass spectrometer and a Fourier transform reflection absorption infrared spectrometer (FT-RAIRS). We obtained the binding energy distribution of NH<sub>3</sub> on crystalline ice (CI) and compact amorphous solid water ice by analysing the TPD profiles of NH<sub>3</sub> obtained after depositions on these substrates.

**Results.** In the co-deposition experiments, we observed a significant delay in the desorption and a decrease of the desorption rate of NH<sub>3</sub> when H<sub>2</sub>O is introduced into the co-deposited mixture of NH<sub>3</sub>-<sup>13</sup>CO or NH<sub>3</sub>-CO<sub>2</sub>, which is not the case in the absence of H<sub>2</sub>O. Secondly, we noticed that H<sub>2</sub>O traps roughly 5–9% of the co-deposited NH<sub>3</sub>, which is released during the phase change of water from amorphous to crystalline. Thirdly, we obtained a distribution of binding energy values of NH<sub>3</sub> on both ice substrates instead of an individual value, as assumed in previous works. For CI, we obtained an energy distribution between 3780 K and 4080 K, and in the case of amorphous ice, the binding energy values were distributed between 3630 K and 5280 K; in both cases we used a pre-exponential factor of  $A = 1.94 \times 10^{15} \text{ s}^{-1}$ .

**Conclusions.** From our experiments, we conclude that the behaviour of NH<sub>3</sub> is significantly influenced by the presence of water, owing to the formation of hydrogen bonds with water, in line with quantum calculations. This interaction, in turn, preserves NH<sub>3</sub> on the grain surfaces longer and up to higher temperatures, making it available closer to the central protostar in protoplanetary discs than previously thought. It explains well why the NH<sub>3</sub> freeze-out in pre-stellar cores is efficient. When present along with H<sub>2</sub>O, CO<sub>2</sub> also appears to impact the behaviour of NH<sub>3</sub>, retaining it at temperatures similar to those of water. This may impact the overall composition of comets, particularly the desorption of molecules from their surface as they approach the Sun.

**Key words.** astrochemistry – molecular processes – methods: laboratory: solid state – comets: general – protoplanetary disks – ISM: molecules

## 1. Introduction

Ammonia is one of the six major molecules found in the solid phase in interstellar ices (Boogert et al. 2015). It has been observed in a variety of environments in the universe, including comets (e.g. Poch et al. 2020), star-forming regions (e.g. Fehér et al. 2022), external galaxies (e.g. Gorski et al. 2018), the centre of our Galaxy (e.g. Sandqvist et al. 2017), and in the Solar System planets. It was first detected in the interstellar medium towards the Galactic centre by Cheung et al. (1968) through its  $J = 1, K = 1$  inversion transition. In dense starless clouds, where temperatures can be as low as 6 K (Crapsi et al. 2007; Paganì et al. 2007) and number densities between  $10^4$  and  $10^6 \text{ cm}^{-3}$  (Keto & Caselli 2010), molecular gas tracers such as CO and CS are depleted from the gas phase and mainly reside on the surface of dust grains upon freeze-out (Caselli et al. 1999;

Tafalla et al. 2002). A similar scenario (large degree of C-bearing molecular freeze-out) is expected in the mid-plane of protoplanetary discs, where number densities are orders of magnitude larger than the central regions of dense starless cores (Dutrey et al. 1997; Henning & Semenov 2013; Qi et al. 2013). However, N-bearing molecules, in particular, NH<sub>3</sub> and N<sub>2</sub>H<sup>+</sup> and their deuterated forms, appear to be more resilient to freeze-out (e.g. Caselli et al. 2002, Tafalla et al. 2002, 2004, Crapsi et al. 2007). For this reason, they are considered to be excellent tracers of dense and cold interstellar regions. More recent work using multi-transition studies done with the IRAM 30 m antenna and high sensitivity interferometric observations with ALMA and JVLA has shown that these molecules freeze out within the central region of pre-stellar cores (e.g. Redaelli et al. 2019; Caselli et al. 2022; Pineda et al. 2022), although at higher densities than CO. Gas-grain astrochemical models are now able

to reproduce the observations (Caselli et al. 2022; Pineda et al. 2022). Still, they are limited by uncertainties in such factors as the binding energies of  $\text{NH}_3$  and knowledge of its surface chemistry. Following the work of Collings et al. (2004), Penteado et al. (2017) derived binding energies for several species, including  $\text{NH}_3$ . Similarly, Collings et al. (2004), He et al. (2016), and Suhasaria et al. (2015) have studied the desorption properties of  $\text{NH}_3$  from various substrates. However, the binding energies of  $\text{NH}_3$ , the importance of surface chemistry for its formation, and its chemical desorption efficiency (Caselli et al. 2017; Sipilä et al. 2019) can still be better constrained.

Kruczkiewicz et al. (2021) has shown that ammonia can be efficiently stored in the form of ammonium salts, which at higher temperatures decompose to release ammonia into the gas phase irrespective of the presence or absence of water. This release into the gas phase occurs at a temperature higher than that of the desorption of water ice ( $T \sim 154\text{ K}$ ) but lower than room temperature. This implies that ammonia could be found closer to a young stellar object than the water snow line. The majority of  $\text{NH}_3$  in molecular mantles should therefore be free to interact with the major components of interstellar or cometary ices such as water,  $\text{CO}_2$ , or  $\text{CO}$ . Similarly, Poch et al. (2020) have demonstrated that ammonium salts are a dominant nitrogen reservoir on cometary surfaces, explaining the low measured cometary nitrogen-to-carbon ratio as compared to that of the Sun. Finally, as ammonia ice is one of the major nitrogen reservoirs in star-forming regions (Öberg et al. 2011), knowledge of the ammonia snow line is crucial when considering the formation and evolution of more complex N-bearing species in planetary systems.

The aim of this work is to study the behaviour of ammonia in the presence of different components of molecular ice mantles, such as  $\text{H}_2\text{O}$ ,  $\text{CO}$ , and  $\text{CO}_2$ . We therefore performed studies to obtain the binding energy of ammonia on different water ice substrates, namely, compact amorphous solid water ice (c-ASW) and crystalline ice (CI). Additionally, we conducted experiments to determine the snow line of ammonia. The article is organised as follows: Sect. 2 describes the experimental set-up; Sect. 3 details the experiments and the results; Sect. 4 discusses the conclusion.

## 2. Experimental set-up

The experiments were performed on the VENUS (VErs de NoUvelles Syntheses) set-up, which allowed us to reproduce the conditions in cold, dark clouds (Congiu et al. 2020). The VENUS set-up consists of an ultra-high vacuum (UHV) chamber that can attain a base pressure of  $1 \times 10^{-10}$  hPa (1 hPa = 1 mbar) and five independent beams (which can be used simultaneously to inject the desired species). A quadrupole mass spectrometer (QMS) and the beam of a Fourier transform reflection absorption infrared spectrometer (FT-RAIRS) were also present in the UHV chamber (hereafter referred to as the main chamber) and could be used to make qualitative and quantitative measurements during the experiments. Depositions were made on a polycrystalline gold substrate enclosed within the main chamber. The substrate is chemically inert and acted as a proxy surface to dust grains for species adsorption and desorption for reactions. This surface was attached to the cold head of a closed-cycle He cryostat, which allowed the surface temperature to be varied between 10 K and 400 K. Four of the five beams were separated from the main chamber via two intermediary chambers. These intermediary chambers were responsible for regulating the pressure of the

injected species between the four beams ( $p \sim 10^{-5}$ – $10^{-4}$  mbar) and the main chamber via differential pumping. The four beams were labelled as follows: top beam, central beam, right beam, and bottom beam. For the experiments in this paper, only the first three beams were used. The fifth beam was attached to the main chamber and could be used to inject species directly into the chamber (also known as ‘background deposition’).

## 3. Results

### 3.1. Co-deposition experiments

Our initial set of experiments were aimed at understanding the interaction of ammonia with the major components found on grain mantles. Our work considers three major molecules:  $\text{H}_2\text{O}$ ,  $\text{CO}$ , and  $\text{CO}_2$ . However, for our experiments, we used  $^{13}\text{CO}$  (mass = 29 amu) instead of  $^{12}\text{CO}$  (mass = 28 amu) to allow for a clear distinction from atmospheric  $\text{N}_2$  (mass = 28 amu) by the QMS. Similarly, the major mass channels for water and  $\text{NH}_3$  are 18 amu and 17 amu, respectively. Water also has fragments of mass equal to 17 amu, and  $\text{NH}_3$  fragments into mass of 16 amu. To distinguish between these overlapping fragments of  $\text{H}_2\text{O}$  and  $\text{NH}_3$ , we performed experiments using each species separately, determined the ratio (percentage) of fragmentation into each mass by the QMS, and calibrated the quantities for each mass proportionately. Initially, we co-deposited ammonia with each of these components separately. We injected the species onto the gold substrate, which was maintained at a temperature of 10 K during the deposition. Each of these species was dosed using separate beams. A laser beam was used to ensure that every beamline overlapped on the same spot on the deposition substrate. The details of the alignment process can be found in Congiu et al. (2020) and have been omitted here for brevity. The pressure of the  $\text{NH}_3$ ,  $^{13}\text{CO}$ , and  $\text{CO}_2$  at the first stage of the beam was a few  $10^{-5}$  mbar (corresponding to a flux:  $0.1\text{ sccm}^1$ ), while that of  $\text{H}_2\text{O}$  was roughly  $4.8 \times 10^{-5}$  mbar. We defined a monolayer as  $1 \times 10^{15}$  molecules  $\text{cm}^{-2}$ . The reproducibility between two depositions is within a few percent, and the accuracy in the absolute determination of an ML is around 20%, as it is more precise for some molecules and less for other species (such as  $\text{NH}_3$ ). Table 1 lists the experiments used for the co-deposition experiments along with the ratios and monolayers of each species used. The raw data (mass spectra as well as IR spectra) are accessible online via a dedicated database<sup>2</sup>. We also carried out and analysed other sets of experiments under similar conditions. These experiments are listed in Appendix A and should be accessible online. For this article, we selected the experiments that best demonstrate our findings.

The inset in Fig. 1 represents the TPD of 1 ML  $\text{NH}_3$  on a gold substrate maintained at 10 K and was used to calibrate all the experiments. In the calibration experiment, to determine the dose for 1 ML, we performed a series of TPDs with various doses of  $\text{NH}_3$  on a gold substrate held at 10 K and a flux of  $0.1\text{ sccm}$  in the injection chamber. We found that 1 ML of  $\text{NH}_3$  is deposited after approximately 9 min of deposition. The ramp for all the experiments was  $0.2\text{ K s}^{-1}$ . The details of the calibration can be found in Appendix B.

Figure 1 shows the TPD curves of the  $\text{NH}_3$ – $\text{H}_2\text{O}$  co-deposition experiments. In the calibration experiment, we observed a sudden rise in the  $\text{NH}_3$  desorption around 80 K,

<sup>1</sup> sccm = standard cubic centimetre.

<sup>2</sup> <https://lerma.labo.cyu.fr/DR/traitement.php>

**Table 1.** Co-deposition experiments.

No.	Experiment	Ratio	Quantity deposited (ML)
1	{NH <sub>3</sub> + H <sub>2</sub> O}	1:1	~10 ML of each
2	{NH <sub>3</sub> + H <sub>2</sub> O}	1:4	5.8 (NH <sub>3</sub> ), 23.8(H <sub>2</sub> O)
3	{NH <sub>3</sub> + <sup>13</sup> CO}	1:1	11.3(NH <sub>3</sub> ), 12.3( <sup>13</sup> CO)
4	{NH <sub>3</sub> + <sup>13</sup> CO}	1:6	1(NH <sub>3</sub> ), 6.5( <sup>13</sup> CO)
5	{NH <sub>3</sub> + <sup>13</sup> CO + H <sub>2</sub> O}	1:1:1	8.1(NH <sub>3</sub> ), 9.2( <sup>13</sup> CO), 9.2(H <sub>2</sub> O)
6	{NH <sub>3</sub> + <sup>13</sup> CO + H <sub>2</sub> O}	1:2:9	1.6(NH <sub>3</sub> ), 3.6( <sup>13</sup> CO), 8.9(H <sub>2</sub> O)
7	{NH <sub>3</sub> + CO <sub>2</sub> }	1:1	14.7(NH <sub>3</sub> ), 14.7(CO <sub>2</sub> )
8	{NH <sub>3</sub> + CO <sub>2</sub> }	1:7	0.7(NH <sub>3</sub> ), 5.4(CO <sub>2</sub> )
9	{NH <sub>3</sub> + CO <sub>2</sub> + H <sub>2</sub> O}	1:1:1	9(NH <sub>3</sub> ), 9.3(CO <sub>2</sub> ), 8.9(H <sub>2</sub> O)
10	{NH <sub>3</sub> + CO <sub>2</sub> + H <sub>2</sub> O}	1:4:5	1.5(NH <sub>3</sub> ), 4(CO <sub>2</sub> ), 5.5(H <sub>2</sub> O)

**Note:** All experiments were performed on a gold substrate held at 10 K. The ratios have been rounded off to the nearest whole number for visual convenience, while the number of monolayers deposited is mentioned to one decimal point of accuracy. The ramp during the TPD was  $0.2 \text{ K s}^{-1}$ . Additional experiments were carried out but are not included in the main article for brevity and can be found in Appendix A.1.

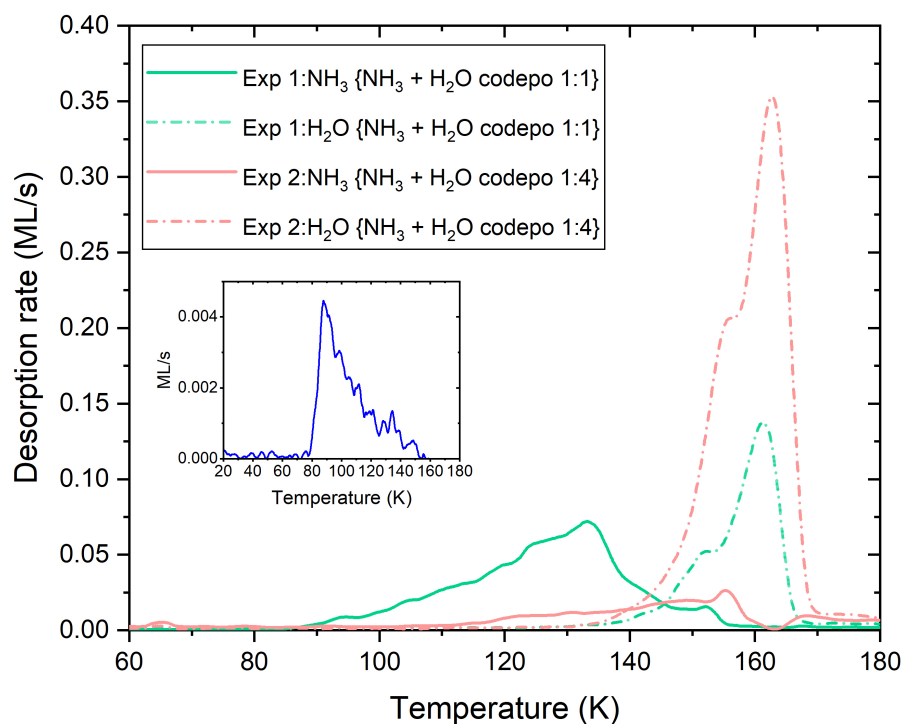


**Fig. 1.** NH<sub>3</sub>–H<sub>2</sub>O co-deposition experiments. All experiments were performed on a gold substrate. The TPDs had a ramp of  $0.2 \text{ K s}^{-1}$ . The solid lines represent the desorption of NH<sub>3</sub>, while the dashed-dotted lines represent the desorption of water. Lines of the same colour belong to the same set of experiments. Inset: TPD of NH<sub>3</sub> from a gold surface used to calibrate all the subsequent experiments.

which falls off slowly once peak desorption has been completed. Contrarily, during the co-deposition with water, we observed a significant decrease of the NH<sub>3</sub> desorption rate, and peak desorption shifted to higher temperatures. We found that about 6% of the deposited NH<sub>3</sub> with regard to H<sub>2</sub>O was trapped by water and then released during the phase change of water from an amorphous to crystalline form. This trapped fraction was estimated

by calculating the area under the TPD profile of the desired species (in this case NH<sub>3</sub>). In reality, water deposited at such a low temperature is fairly porous and, hence, has a larger surface area wherein the NH<sub>3</sub> molecules can lodge themselves. As the temperature was raised, water underwent a phase change from amorphous to crystalline form, which can be observed through the plateau or “shoulder” at around 155 K in the desorption

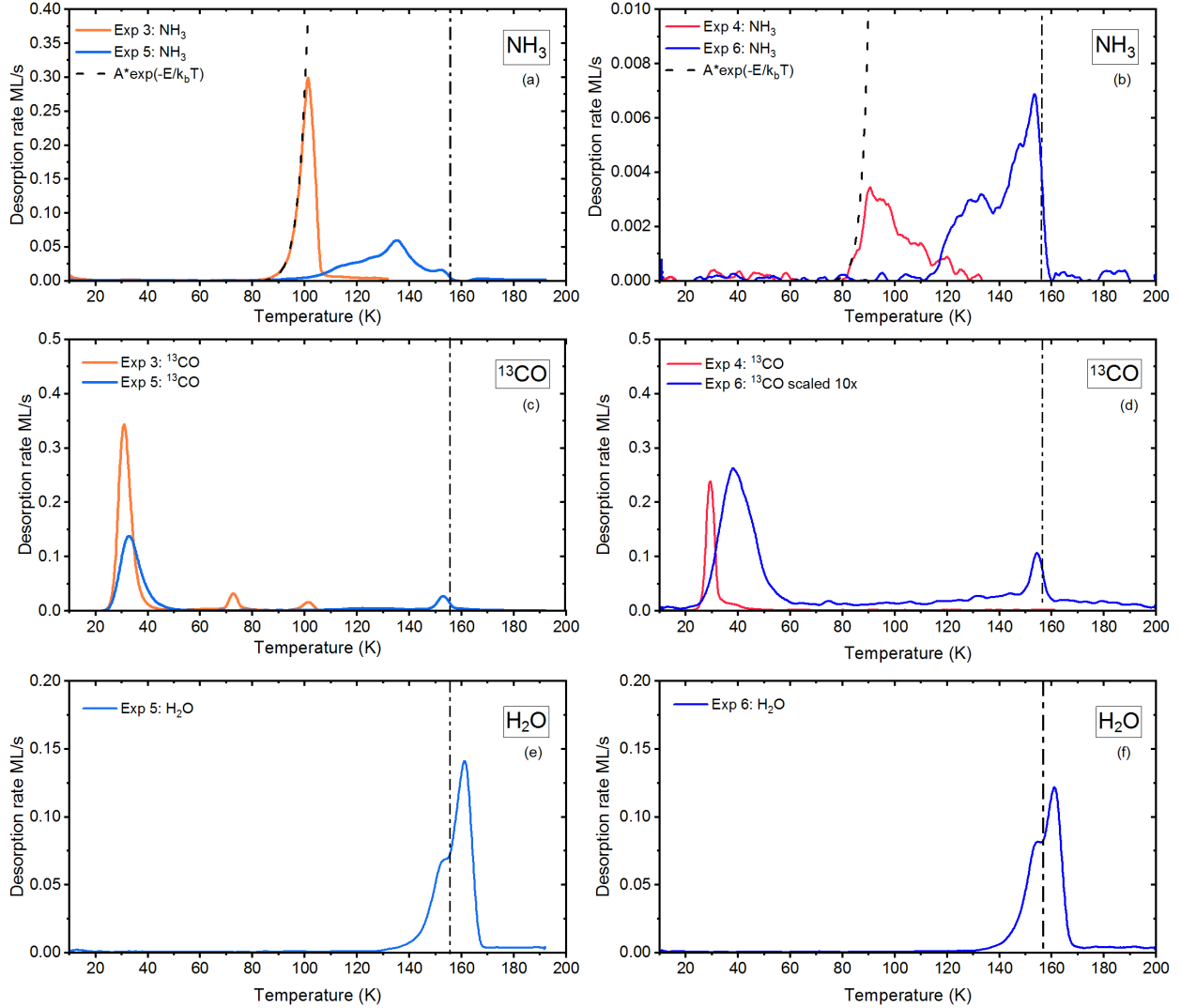


**Fig. 2.**  $\text{NH}_3$ - $^{13}\text{CO}$  (and  $\text{H}_2\text{O}$ ) co-deposition experiments. The mass channels used for  $\text{H}_2\text{O}$ ,  $\text{NH}_3$ , and  $^{13}\text{CO}$  are 18 amu, 17 amu, and 29 amu, respectively, also accounting for fragments of mass = 17 amu (for  $\text{H}_2\text{O}$ ) and 16 amu (for  $\text{NH}_3$ ). All experiments were performed on a gold substrate. The TPDs have a ramp of  $0.2 \text{ K s}^{-1}$ . Lines of the same colour belong to the same set of experiments. The dash-dot vertical line at 155 K corresponds to the temperature of the phase change of water from amorphous to crystalline.

curve of water (Fig. 1; see also Speedy et al. 1996) as well as a change in the IR spectra (not shown here). During this phase change, water molecules began to re-arrange to form a crystalline structure, during which any  $\text{NH}_3$  in its bulk was pushed out. Furthermore, the higher the  $\text{H}_2\text{O}/\text{NH}_3$  ratio, the more the desorption of ammonia was delayed – as expected. Indeed, when the  $\text{NH}_3$  concentration was very high, there were more  $\text{NH}_3$ - $\text{NH}_3$  interactions that could substitute for  $\text{NH}_3$ - $\text{H}_2\text{O}$  interactions.

During the TPD of the co-deposition experiments of  $\text{NH}_3$ - $^{13}\text{CO}$  mixture (Fig. 2),  $\text{NH}_3$  desorbs independently (top row Fig. 2a and b) of  $^{13}\text{CO}$ , irrespective of the ratio between the two. All of the  $\text{NH}_3$  was desorbed between 80 K and 132 K. The desorption is in good agreement with a fit to the desorption rate equation  $A \times \exp(-E/k_b T)$ , where  $E/k_b$  is the binding energy (in Kelvins),  $T$  is the temperature (in Kelvins), and  $A$  is the pre-exponential factor ( $\text{s}^{-1}$ ). Since our experiments are in the multilayer regime (zero order kinetics), we chose  $E/k_b = 2965 \text{ K}$  and the  $A = 2.1 \times 10^{12} \text{ s}^{-1}$  following Martín-Doménech et al. (2014) and assuming that  $1 \text{ ML} = 10^{15} \text{ molecules cm}^{-2}$ . The offset from the fit seen in Fig. 2b is due to the low quantities of

$\text{NH}_3$  used for the experiments. Higher quantities would ensure a good fit, as in the previous case.

When present with  $\text{NH}_3$  in equal quantities, 85.8% of the deposited  $^{13}\text{CO}$  is desorbed between 20 K and 50 K (Fig. 2c, middle row, orange curve). At the same time,  $^{13}\text{CO}$  exhibits a volcano effect due to  $\text{NH}_3$ . A volcano effect is the sudden desorption of a volatile species trapped under a less volatile species, such as  $\text{H}_2\text{O}$ , when the latter begins to desorb (Smith et al. 1997; Viti et al. 2004; Collings et al. 2003). This volcano effect can be observed through the peak between 68 K and 80 K, and it accounts for approximately 9% of the total desorbed  $^{13}\text{CO}$ . This trapping is not observed when  $\text{NH}_3$  is present in trace quantities, as expected (Fig. 2d). The  $^{13}\text{CO}$  peak between 90 K and 110 K is the  $\text{CO}$  desorbing with  $\text{NH}_3$ . This is probably the  $\text{CO}$  being adsorbed on the substrate during the initial moments of the co-deposition and thereby becoming buried under the later layers of  $\text{NH}_3$  and  $^{13}\text{CO}$ . The right panels of Fig. 2 contain the experiments in proportions that are more astronomically relevant. Hence, there,  $\text{NH}_3$  is deposited in trace amounts (1 ML or sub-monolayer quantities) as compared

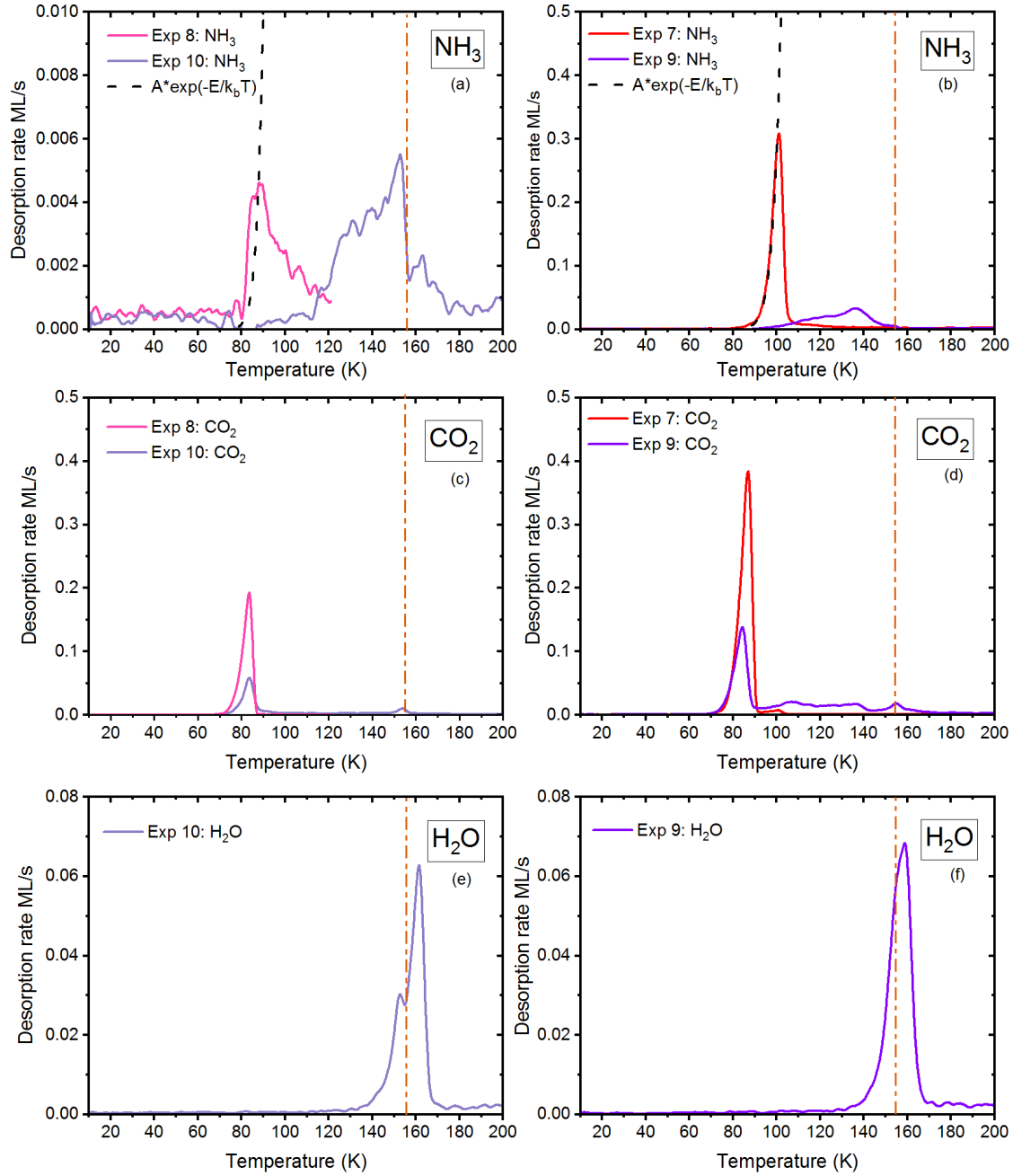


**Fig. 3.** Same as Fig. 2 but using  $\text{CO}_2$  instead of  $^{13}\text{CO}$ . The mass channel used for  $\text{CO}_2$  is 44 amu.

to  $^{13}\text{CO}$  and  $\text{H}_2\text{O}$ . Once again, for  $\text{NH}_3$ , we observed a similar desorption trend as in the case of the experiments presented in Fig. 1.

In the presence of  $\text{H}_2\text{O}$ , the trend in the desorption of  $\text{NH}_3$  and  $^{13}\text{CO}$  is different, as a significant delay in the desorption of  $\text{NH}_3$  was observed. When present in quantities roughly equal to water, the  $\text{NH}_3$  desorption rate is slower, and the desorption is delayed compared to its desorption in the absence of water. In the multi-layer (Fig. 2a) and the sub-monolayer (Fig. 2b) scenarios, the  $\text{NH}_3$  desorption is shifted to higher temperatures. In the former,  $\text{NH}_3$  desorption is delayed, possibly because it needs to diffuse through the bulk of the ice before desorption can take place. In the latter, at low concentrations, there is a higher probability for greater  $\text{NH}_3$ – $\text{H}_2\text{O}$  interaction and lower

$\text{NH}_3$ – $\text{NH}_3$  interaction via hydrogen bonds, resulting in water holding on to  $\text{NH}_3$  for a little longer than when  $\text{NH}_3$  is present in larger quantities. We find it is worth noting that in both cases, an  $\text{NH}_3$  volcano peak was observed due to the crystallisation of water. Roughly 5% of  $\text{NH}_3$  with regard to water is trapped by water when co-deposited in equal quantities, and around 8.5% is trapped by water in the more astronomically relevant scenario (Expt 6 in Table 1) where it is released, as observed in previous experiments, during the  $\text{H}_2\text{O}$  change of phase from amorphous to crystalline.

The co-deposition experiments of  $\text{NH}_3$  with  $\text{CO}_2$  also exhibited a similar behaviour as experiments with  $\text{CO}$ . The  $\text{NH}_3$  desorption appears to be unaffected by the presence of  $\text{CO}_2$  (Figs. 3a and b), as  $\text{NH}_3$  desorbed in the same temperature range

as previously observed for experiments with  $^{13}\text{CO}$ . Its desorption fits well with the curve of the desorption rate equation mentioned earlier with the values taken from [Martín-Doménech et al. \(2014\)](#). When  $\text{NH}_3$  and  $\text{CO}_2$  are in equal quantities (Fig. 3b), the bulk of  $\text{CO}_2$  desorbs between 70 K and 92 K. Of the deposited  $\text{CO}_2$ , 2% desorbs during the desorption of  $\text{NH}_3$ . This could be due to mechanical trapping by  $\text{NH}_3$ , and hence the former may be able to desorb only after all the  $\text{NH}_3$  has desorbed. The shift in peak desorption temperature of  $\text{NH}_3$  towards higher values as observed in Fig. 3b when compared to Fig. 3a is due to the fact that in the former, we had multiple layers of  $\text{NH}_3$ . Additionally, in the sub-ML experiments (Figs. 3a, c and e), we used very low quantities of  $\text{NH}_3$ , and therefore, the interaction between  $\text{NH}_3$  and the gold in the substrate became significant. Once again, the presence of  $\text{H}_2\text{O}$  seems to significantly alter the desorption of both  $\text{NH}_3$  (Figs. 3a and b) and  $\text{CO}_2$  (Figs. 3c and d). The  $\text{NH}_3$  desorbed in a similar manner to the previous experiments with  $^{13}\text{CO}$ . Its desorption was not only delayed, but the rate was also slower. Roughly 9% of it was trapped and then later released during the phase change of  $\text{H}_2\text{O}$ . The  $\text{CO}_2$  desorption, on the other hand, does not appear delayed. However, roughly 2% of it was trapped by water and then released along with  $\text{NH}_3$  during the phase change of  $\text{H}_2\text{O}$ . In previous experimental works, [Bossa et al. \(2008\)](#) and [Noble et al. \(2014\)](#) have shown that carbamic acid ( $\text{NH}_2\text{COOH}$ ) can be formed as early as 80 K by thermal reaction of  $\text{CO}_2$  and  $\text{NH}_3$ . We did not observe this reaction in our experiments, which were performed in much thinner layers, probably because this reaction only occurs if the reactants are solvated. Similarly, [Potapov et al. \(2019\)](#) reported the formation of  $\text{NH}_4^+\text{NH}_2\text{COO}^-$ , which we did not observe in our experiments either.

### 3.2. Desorption of $\text{NH}_3$ from different types of ices

A second set of experiments was performed to understand the desorption dynamics and determine the distribution of binding energies. The method used has been discussed in more detail in [De Jong & Niemantsverdriet \(1990\)](#), [He et al. \(2011\)](#), and [Amiaud \(2006\)](#). Subsequent depositions of roughly 1 ML of  $\text{NH}_3$  were made on each type of ice substrate followed by a TPD. Two kinds of ice substrates were used for this purpose: CI and c-ASW. The CI substrate was formed by depositing water onto the deposition surface held at 110 K followed by flash heating up to 150 K. To create a c-ASW substrate, water was deposited onto the gold substrate at 110 K and an incident angle of  $\theta = 0^\circ$  with respect to the normal angle of the gold substrate. A normal angle of incidence leads to a denser ice substrate, as shown by [Kimmel et al. \(2001a,b\)](#). Several studies have shown a key role between the deposition temperature and its effect on the ice substrate. [Scott Smith et al. \(2006\)](#) found that water deposited at  $\leq 110$  K is amorphous but already begins to pre-crystallise at  $\geq 120$  K since this state is thermodynamically favoured. [He et al. \(2019\)](#) and [Bossa et al. \(2012\)](#) observed a significant reduction in the porosity of the substrate beyond 100 K. These studies were performed on samples that are  $\sim 200$  MLs and  $\sim 3000$  MLs, respectively, while our present study focuses on thin ices ( $\sim$ tens of monolayers). Hence, it is safe to assume that the amorphous substrate formed in our case is indeed compact.

To prepare the raw data for analysis, an initial adjacent averaging smoothing process employing 35 data points was applied using Origin software. This initial smoothing was carried out to reduce background noise, which becomes significant at low dosages and high temperatures. Subsequently, the smoothed data was fed into a custom software developed at LERMA, which fits

a set of 19 independent TPD curves distributed evenly over a range of 19 binding energies spanning from 3030 K to 5730 K. For a more comprehensive explanation of this method, we refer to [Chaabouni et al. \(2018\)](#). In our analysis, we used a pre-exponential factor,  $A$ , with a value of  $1.94 \times 10^{15} \text{ s}^{-1}$ , as per the findings in Table 2 of [Minissale et al. \(2022\)](#). The results are presented in the form of blue curves, representing the mass spectrometer data, and orange curves, representing the fit to the experiments conducted using software developed within our laboratory.

As Fig. 4 shows,  $\text{NH}_3$  on CI desorbs in a manner similar to  $\text{NH}_3$  on the gold substrate just as in the calibration experiments. There is a sharp increase in the desorption rate at 75 K. Most of the desorption occurs between 78 K and 140 K. On CI, we observed two peaks. The first one (between 76 K and 98 K) is the multi-layer desorption of  $\text{NH}_3$  due to its interaction with itself rather than with the surface, and it does not necessarily need full layers of  $\text{NH}_3$  to be present to appear. The second is between 98 K and 112 K, and we observed an increase in the height of this peak with each deposition. This implies that the surface evolves with each cycle of dosing the crystalline surface with  $\text{NH}_3$ . In other words,  $\text{NH}_3$  is able to amorphise the surface structure of the ice by introducing defects onto its surface. This modification seems, however, to be a surface phenomenon and alters only the top layers of the surface. Even when the quantity of  $\text{NH}_3$  is increased,  $\text{NH}_3$  prefers to bind to  $\text{H}_2\text{O}$  than with itself, as evidenced by the observed increase in peak height in Fig. 4. Nevertheless, this modification does not affect the desorption of either  $\text{H}_2\text{O}$  or  $\text{NH}_3$ , as the latter is eventually pushed out of the surface of CI during the desorption of water. This, in turn, renders it harder to calculate one single value of binding energy for  $\text{NH}_3$  on CI.

[He et al. \(2016\)](#) conducted a similar investigation in which they deposited  $\text{NH}_3$  onto a CI substrate to determine the binding energy of  $\text{NH}_3$  desorption. Our study exhibits considerable resemblance with their research, particularly with respect to their TPD curve obtained for a deposition of 2 ML. Noticeably, a major proportion of the desorption events in both studies occur within the temperature range of 80 K to 145 K. However, a discrepancy arises in the temperature at which the multi-layer desorption peak is observed. He et al. reported this peak as occurring at a slightly elevated temperature, approximately 100 K. This difference could potentially be attributed to their use of a higher heating ramp rate, estimated to be around  $0.5 \text{ K s}^{-1}$ , during their TPD experiments. Another distinguishing feature between the two studies pertains to the temperature of complete desorption of the ices. In our investigation, we observed that the ices are nearly completely desorbed by 140 K, whereas [He et al. \(2015\)](#) noted the presence of desorption signals persisting beyond 140 K. Unfortunately, a more comprehensive comparison is hindered by a lack of specified units for the desorption rate in the pertinent figure within their study. But the difference in heating speed is certainly the main difference since the slower the heating, the earlier the desorption for an equivalent quantity. In terms of the determination of binding energies, [He et al. \(2015\)](#), adopting the direct inversion method, reported binding energy values falling within the range of approximately 2900 K to 4100 K. Notably, these binding energy values are lower than the values obtained in our study. This variance in binding energy values may be attributed to the use of a lower pre-exponential factor, specifically  $10^{12} \text{ s}^{-1}$ , in their methodology as compared to the one employed in our study where we use the conversion formula proposed in [Chaabouni et al. \(2018\)](#) and reported in the review of [Minissale et al. \(2022\)](#).

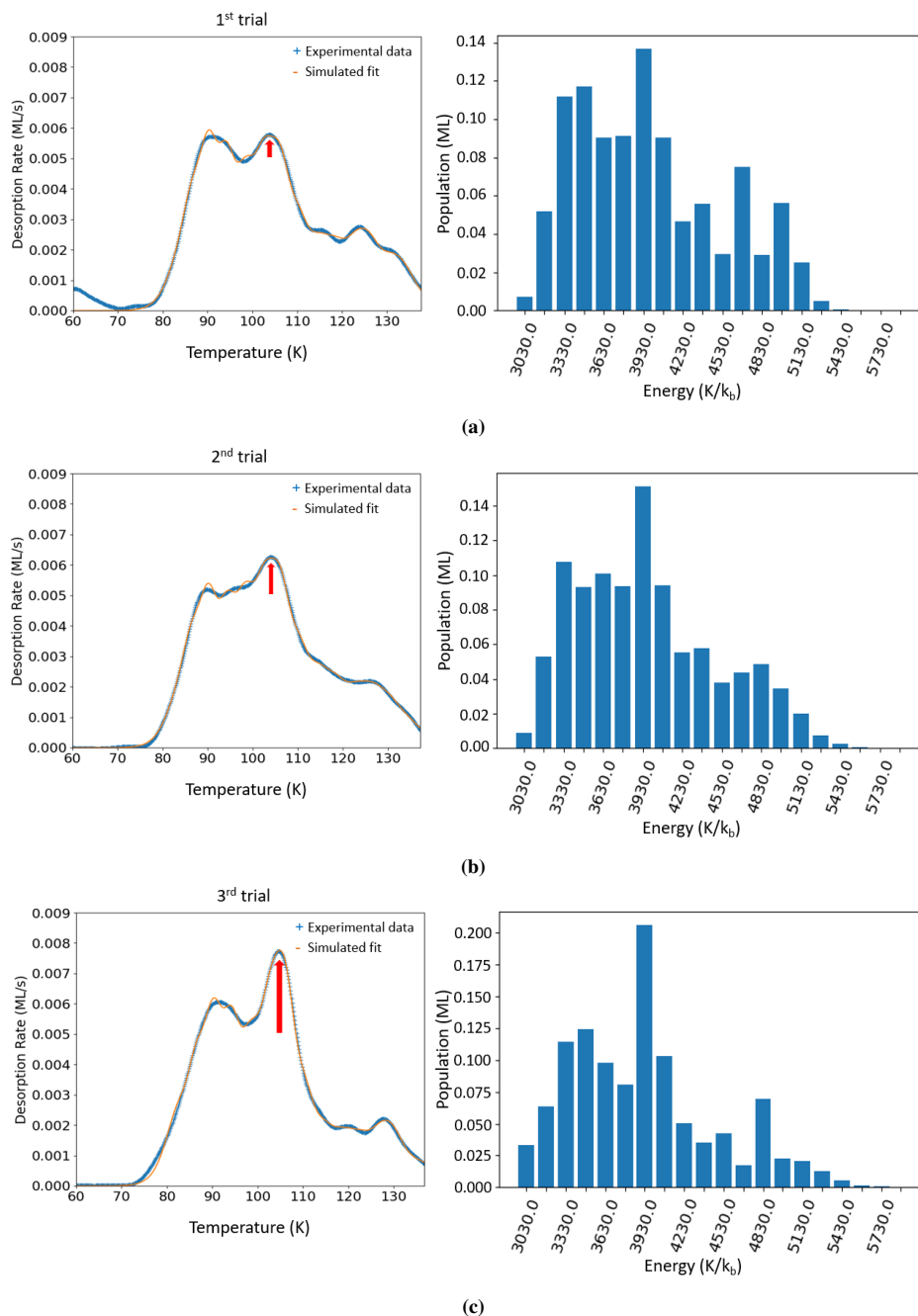


**Fig. 4.** Binding energy fits of the TPDs (*left column*) and the corresponding binding energy distribution histograms (*right column*) of three separate, subsequent depositions of 1 ML of  $\text{NH}_3$  on the surface of CI. Each deposition is followed by a TPD to remove the ammonia deposited on the ice substrate before the subsequent deposition was made. The preference of ammonia to bind to water instead of itself can be seen through the progressive increase in peak height (indicated by the red arrow) with each trial.

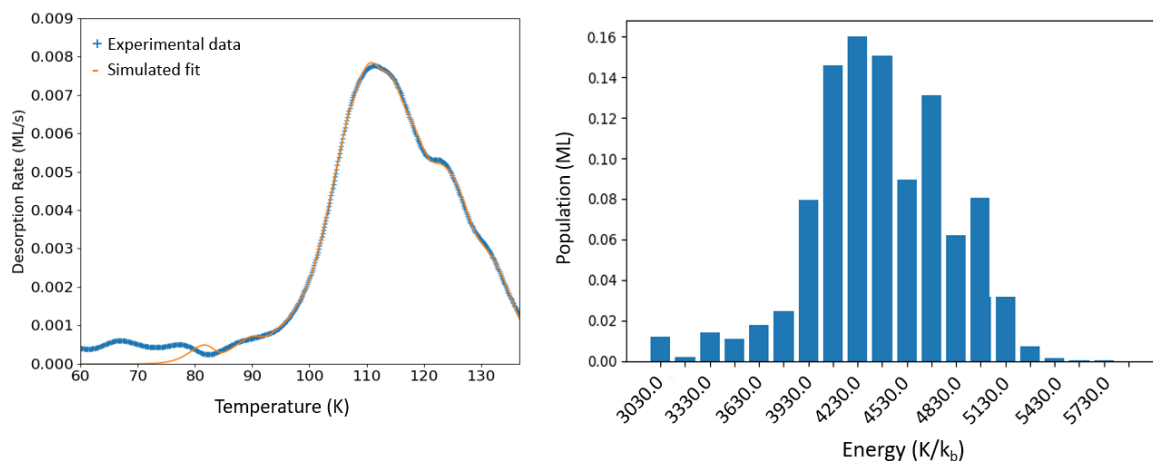
In contrast, the desorption of  $\text{NH}_3$  on c-ASW (Fig. 5) occurs at higher temperatures. This delay could be associated with the structure of c-ASW, that is, due to the presence of concavities at the molecular level on its surface where  $\text{NH}_3$  can lodge itself and be surrounded by many water molecules and hence form more hydrogen bonds than in the case of CI. We observed a single broad peak, which is in contrast to what we observed with CI. A bulk of this desorption occurred between 95 K and 140 K. On CI, we obtained the binding energy between two monolayers of ammonia in the range of 3180–3630 K and between ammonia and the surface of the water substrate in the range of 3780–4080 K. On c-ASW, we obtained binding energy values between 3630 K and 5280 K. Our binding energy values are in

very good agreement with the values obtained for ASW ice via theoretical calculations by Tinacci et al. (2022), who also used the same value of the pre-exponential factor. We also note that in experiments as well as calculations, binding energy distributions are important and have a very good match with Germain et al. (2022). A more detailed discussion between the comparison of experiments and calculations derived values can be found in Ferrero et al. (2022).

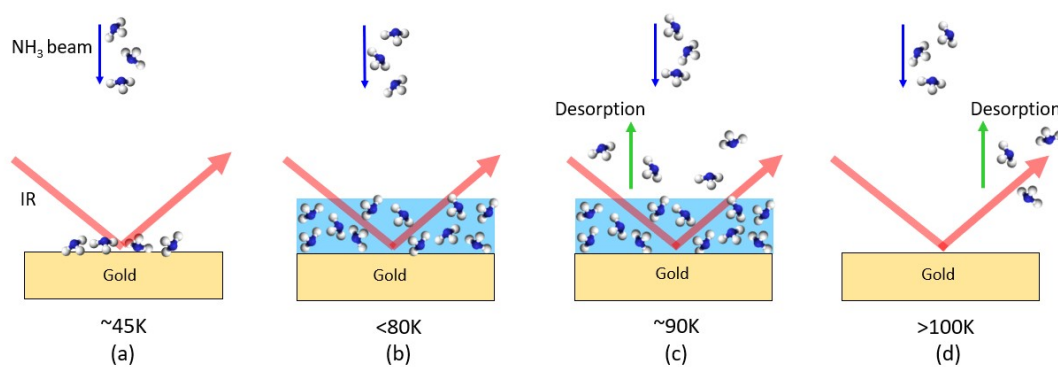
### 3.3. Temperature programmed-during exposure desorption experiments

Figure 6 shows the basic schematics of a TP-DED experiment using the example of pure  $\text{NH}_3$  deposition. For this set of





**Fig. 5.** Binding energy fit (*left panel*) for 1 ML deposition of  $\text{NH}_3$  on c-ASW ice and the corresponding binding energy histogram (*right panel*).



**Fig. 6.** Schematic explaining the sequence of events in the TP-DED experiment. Here, we used the example of an  $\text{NH}_3$  beam, but the same procedure follows for all three TP-DED experiments performed in this work. The temperatures in each sub-figure in the schematic are merely indicative due to the flux dependence of the adsorbate and do not represent the unique temperature at which the events take place.

experiments, the desired species is deposited onto the gold substrate (Fig. 6a) while the latter is simultaneously heated or cooled at a constant ramp of  $0.5 \text{ K min}^{-1}$ . During the heating process, as the deposition progresses, the species continues to accumulate or adsorb on the substrate (Fig. 6b) until the desorption temperature range of the former is reached. At this point, the species begins to slowly desorb from the substrate, and any incoming molecule of the species desorbs immediately (Fig. 6c) until no more incoming molecules can adsorb due to the temperature of the surface being higher than the desorption temperature (Fig. 6d). The reverse occurs during the cooling process. The experiment was monitored using the FT-RAIRS during the deposition and was usually followed by a TPD at the end. The details of each experiment are given in Table 2. The aim of this rather rarely used type of experiment was to mimic snow line regions where both accretion and depletion on grains (i.e. sticking and desorption) take place simultaneously. A snow line is defined in a region with a thermal gradient that applies on the grains (i.e. hotter towards the star and cooler in the outer regions) such that there exists a frontier zone (the snow line) where the accretion compensates for the desorption. Towards the colder side, the accretion dominates and the molecules condense onto the grains, whereas on the hotter side, the concerned species are in a gas phase. We emphasise that our goal was to investigate the snow line of  $\text{NH}_3$ . The results of the experiments can be found in Fig. 7.

Our study plots the area under the IR peak at  $3383 \text{ cm}^{-1}$  of  $\text{NH}_3$  against temperature. The areas were calculated using

**Table 2.** TP-DED experiments.

Expt No.	Adsorbate	Temperature range (K)
1	$\text{NH}_3$	40–105
		105–94
2	$\text{NH}_3 + \text{H}_2\text{O}$	40–180
		180–60
3	$\text{NH}_3 + \text{H}_2\text{O} + \text{CO}_2$	40–180

the vibrational spectroscopy software OPUS by the company BRUKER. We applied a baseline correction where necessary. We find it important to mention that in experiments two and three, due to heavy baseline distortion and the fact that the IR peaks of  $\text{NH}_3$  were superimposed with that of  $\text{H}_2\text{O}$ , we were obliged to make gross assumptions in order to obtain the IR area of  $\text{NH}_3$ . Hence, the area we report on is the area of  $\text{NH}_3$  subtracted from the combined areas of  $\text{NH}_3$  and  $\text{H}_2\text{O}$ .

All three experiments (see Figs. 7a–c) show distinct zones during the TP-DED. In the first experiment (Fig. 7a), Zone A corresponds to the accretion of  $\text{NH}_3$  in the amorphous form. Given the time to form 1 ML on the gold substrate, the signal before 60 K corresponds to  $\text{NH}_3$  on the substrate. Beyond this temperature, the observed signal is of  $\text{NH}_3$  on this  $\text{NH}_3$  layer.

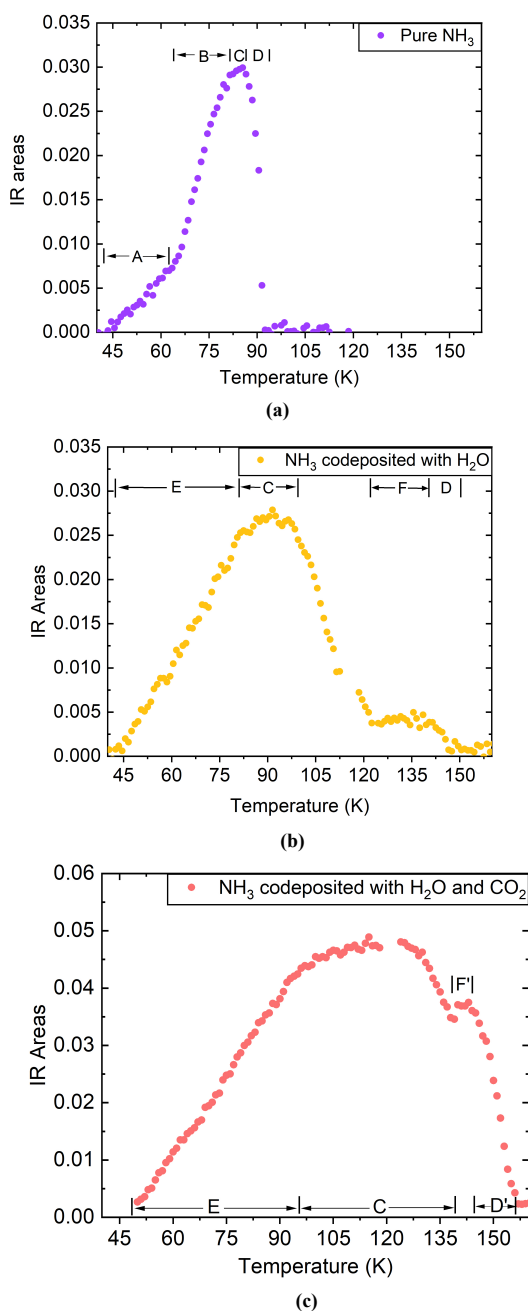


**Fig. 7.** Figure depicting the quantity of NH<sub>3</sub> deposited with respect to temperature (K) during the TP-DED experiments, measured using a FT-RAIRS. For details on the zones A, B, C, D, D', E, F, and F', see main text, Sect. 3.3.

Since the surface was continuously exposed to gaseous NH<sub>3</sub> and the desorption was negligible for these temperatures, ammonia accumulated on the surface, and we observed a linear increase in the IR absorbance signal. The same trend would be observed for a constant surface temperature desorption. As the temperature rose, NH<sub>3</sub> began to change its structure from amorphous to crystalline, denoted as Zone B and identifiable by a change in the slope. This was not due to a change in the flux of accretion, which is stable during every experiment, but is due to an increase in the absorption band strength after the phase transition. This phenomenon was also observed in [Cazaux et al. \(2022\)](#), where a similar change was found during the heating of H<sub>2</sub>S.

Around 81.5 K, we noticed a slowing down of the rise followed by a plateau (Fig. 7a, Zone C). Even though the desorption rate of NH<sub>3</sub> increases exponentially, it was in competition with the accretion rate. As a result, a part of the adsorbed molecules was then desorbing, and thus the net accumulation slowed down to almost null at the snow line, which is the turning point of the curve at around 88 K. Above 90 K, we noticed a sudden drop in the NH<sub>3</sub> desorption (Zone D). Here, despite the accretion, desorption still dominates. This occurred since there is no more measurable NH<sub>3</sub> on the surface, as the adsorbed ammonia was desorbed quickly after adsorption, which is even faster in a laboratory measurement time frame.

We then performed a co-deposition of NH<sub>3</sub> with H<sub>2</sub>O (see Fig. 7b) under similar conditions. The first striking observation was the absence of the region of phase change of NH<sub>3</sub> from amorphous to crystalline. This could be due to the aforementioned preference of NH<sub>3</sub> to form hydrogen bonds with H<sub>2</sub>O than with itself. Hence, Zone E could be considered as the region that contains NH<sub>3</sub> within the H<sub>2</sub>O structure. The turn-off point between Zone E and Zone C is less pronounced than in the previous case, and it marks the desorption of NH<sub>3</sub> in interaction with itself and probably not the water ice. After roughly 105 K, there was a decrease in the quantity of NH<sub>3</sub> due to the substrate reaching a higher desorption flux of NH<sub>3</sub>. However, an interesting point to note here is that there was still a significant quantity of NH<sub>3</sub> left on the surface. This can be verified by the plateau (Zone F), which is an indicator of NH<sub>3</sub> in H<sub>2</sub>O. This was due to the trapping phenomena observed earlier by H<sub>2</sub>O, and it was further strengthened by the NH<sub>3</sub>–H<sub>2</sub>O interaction. The slow decrease in the slope in Zone D corresponds to the release of NH<sub>3</sub> due to the desorption of H<sub>2</sub>O as the latter approached its crystallisation temperature.

In the next set of experiments (Fig. 7c), we added CO<sub>2</sub> to this mixture. During the experiment, we perceived a similar trend to that of the previous experiment with H<sub>2</sub>O at the beginning of the desorption process, that is, the sudden change in the curve for NH<sub>3</sub> is very subtle, if at all present (Zone E). The accretion continued until the mixture reached around 97 K. At this temperature, we began to recognise some similarities with the previous two experiments. Firstly, the signal of the solid NH<sub>3</sub> is characterised by a plateau (Zone C) due to the competition between NH<sub>3</sub> accretion and desorption. This plateau was followed by a sudden yet short drop in the quantity of NH<sub>3</sub>, owing to the high temperature. Zone F marks the narrow plateau due to the NH<sub>3</sub>–H<sub>2</sub>O–CO<sub>2</sub> interaction. We find it interesting to note that the quantity of NH<sub>3</sub> (in other words, the IR area) in this zone is significantly higher than in the two previous cases. This could point to an additional interaction of NH<sub>3</sub> with CO<sub>2</sub> that retains NH<sub>3</sub> until a higher temperature. However, the most interesting point to note between all three experiments is the progressive shift in the peak desorption temperature of NH<sub>3</sub> as we added each new species to pure NH<sub>3</sub>, especially in the presence of H<sub>2</sub>O, and even more so with the addition of CO<sub>2</sub>. There is still some NH<sub>3</sub> in the solid phase at unexpectedly high temperatures. In the case of the NH<sub>3</sub>–CO<sub>2</sub>–H<sub>2</sub>O mixture, the snow line (the turning point of NH<sub>3</sub>) coincides with the beginning of the desorption of water, almost superimposing over their snow lines. This also raises a question about the potential role of CO<sub>2</sub> in the desorption of NH<sub>3</sub>. These experiments directly demonstrate that NH<sub>3</sub> lacks a snow line of its own when combined with H<sub>2</sub>O (and potentially CO<sub>2</sub>), which consequently retains the NH<sub>3</sub> molecules on the grain up to higher temperatures than previously expected and, therefore, in a different spatial zone (the same as water).

## 4. Conclusions

Nitrogen-based molecules have been found in the densest parts of the interstellar medium, such as pre-stellar cores, where they freeze out at densities higher than those found for CO and other C-bearing molecules. Therefore, N-bearing molecules are excellent tracers of these dense regions that are otherwise difficult to observe. In this present work, we studied the interactions of NH<sub>3</sub> on grain surfaces – which are still poorly understood – in the presence of other species found on grain surfaces, including H<sub>2</sub>O, CO<sub>2</sub>, and <sup>13</sup>CO. We performed various types of experiments with the four species under conditions that mimicked those found in pre-stellar cores and protoplanetary discs, paying close attention to the behaviour of NH<sub>3</sub> in each case. We also calculated the binding energy of NH<sub>3</sub> on two different types of water substrates: compact amorphous solid water ice (c-ASW) and crystalline ice (CI). The main findings of our study are as follows:

1. During the co-deposition of NH<sub>3</sub> with H<sub>2</sub>O, we observed a delay in the desorption and a lowering of the NH<sub>3</sub> desorption rate. Additionally, H<sub>2</sub>O trapped around 6% of NH<sub>3</sub>, which was then released during the water phase change from amorphous to crystalline. However, when NH<sub>3</sub> was co-deposited with either <sup>13</sup>CO or CO<sub>2</sub>, we observed no such behaviour. This behaviour was observed once again when we added H<sub>2</sub>O to the NH<sub>3</sub>–<sup>13</sup>CO or NH<sub>3</sub>–CO<sub>2</sub> mixture. In the NH<sub>3</sub>–<sup>13</sup>CO–H<sub>2</sub>O and the NH<sub>3</sub>–CO<sub>2</sub>–H<sub>2</sub>O experiments, we observed roughly 5–9% of trapped NH<sub>3</sub> with respect to water, which was then released during the phase change of water from amorphous to crystalline;
2. We note that NH<sub>3</sub> has a range of binding energy values instead of a unique value, in agreement with recent theoretical calculations. For CI, we obtained NH<sub>3</sub>–H<sub>2</sub>O binding energy values in the range of 3780–4080 K. We observed that NH<sub>3</sub> is able to amorphise the substrate surface by disrupting the structural order of the surface of the ice via hydrogen bonding with H<sub>2</sub>O. In the case of c-ASW, we obtained binding energies in the range of 3630–5280 K (for a pre-exponential factor set to  $A = 1.94 \times 10^{15} \text{ s}^{-1}$  in both cases);
3. During the TP-DED experiments, the crystallisation of NH<sub>3</sub> is noticeably impacted in the presence of H<sub>2</sub>O and CO<sub>2</sub>. Furthermore, the desorption temperature of NH<sub>3</sub> increases significantly in their presence, and it desorbs over a longer range of temperatures. There is also some trapping of NH<sub>3</sub> observed during the experiments. This indicates that NH<sub>3</sub> has no definite snow line and seems to be strongly influenced by these species. The trapping enables it to be stored on the dust grains and is thereby available at later times and/or able to be transported to higher temperatures (e.g. closer to the central protostar or towards the inner disc of more evolved young stellar objects) in order to form more complex molecules.

In conclusion, our investigation sheds light on the intricate interactions of NH<sub>3</sub> on grain surfaces, especially in the presence of key species such as H<sub>2</sub>O, CO<sub>2</sub>, and <sup>13</sup>CO. The observed delays in desorption, various binding energies, and the influence of these species on NH<sub>3</sub> crystallization underline the sensitivity of NH<sub>3</sub> to the surrounding molecular environment. These findings contribute valuable insights into the understanding of nitrogen-bearing molecules in dense interstellar regions and their role in the chemical evolution in these regions.

*Acknowledgements.* This work was funded by CY Initiative of Excellence (grant “Investissements d’Avenir” ANR-16-IDEX-0008), Agence Nationale de

la recherche (ANR) SIRC project (Grant ANR-SPV202448 2020-2024), by the Programme National “Physique et Chimie du Milieu Interstellaire” (PCMI) of CNRS/INSU with INC/INP co-funded by CEA and CNES, and by the DIM-ACAV+, a funding programme of the Region Ile de France.

## References

- Amiaud, L. 2006, PhD thesis, Cergy-Pontoise, France
- Boogert, A. A., Gerakines, P. A., & Whittet, D. C. 2015, *A&A*, **53**, 541
- Bossa, B., Theulé, P., Duvernay, F., Borget, F., & Chiavassa, T. 2008, *A&A*, **492**, 719
- Bossa, J.-B., Isokoski, K., De Valois, M., & Linnartz, H. 2012, *A&A*, **545**, A82
- Caselli, P., Walmsley, C., Tafalla, M., Dore, L., & Myers, P. 1999, *ApJ*, **523**, L165
- Caselli, P., Benson, P. J., Myers, P. C., & Tafalla, M. 2002, *ApJ*, **572**, 238
- Caselli, P., Bizzocchi, L., Keto, E., et al. 2017, *A&A*, **603**, A1
- Caselli, P., Pineda, J. E., Sipilä, O., et al. 2022, *ApJ*, **929**, 13
- Cazaux, S., Carrascosa, H., Caro, G., et al. 2022, *A&A*, **657**, A100
- Chaabouni, H., Diana, S., Nguyen, T., & Dulieu, F. 2018, *A&A*, **612**, A47
- Cheung, A. C., Rank, D. M., Townes, C. H., Thornton, D. D., & Welch, W. J. 1968, *Phys. Rev. Lett.*, **21**, 1701
- Collings, M. P., Dever, J. W., Fraser, H. J., McCoustra, M. R., & Williams, D. A. 2003, *ApJ*, **583**, 1058
- Collings, M. P., Anderson, M. A., Chen, R., et al. 2004, *MNRAS*, **354**, 1133
- Congiu, E., Sow, A., Nguyen, T., Baouche, S., & Dulieu, F. 2020, *Rev. Sci. Instrum.*, **91**, 124504
- Crapsi, A., Caselli, P., Walmsley, M. C., & Tafalla, M. 2007, *A&A*, **470**, 221
- De Jong, A., & Niemantsverdriet, J. 1990, *Surf. Sci.*, **233**, 355
- Dutrey, A., Guilloteau, S., & Guélin, M. 1997, *A&A*, **317**, L55
- Fehér, O., Tóth, L. V., Kraus, A., et al. 2022, *ApJS*, **258**, 17
- Ferrero, S., Grieco, F., Ibrahim Mohamed, A.-S., et al. 2022, *MNRAS*, **516**, 2586
- Germain, A., Tinacci, L., Pantaleone, S., Ceccarelli, C., & Ugliengo, P. 2022, *ACS Earth Space Chem.*
- Gorski, M., Ott, J., Rand, R., et al. 2018, *ApJ*, **856**, 134
- He, J., Frank, P., & Vidalí, G. 2011, *Phys. Chem. Chem. Phys.*, **13**, 15803
- He, J., Shi, J., Hopkins, T., et al. 2015, *ApJ*, **801**, 120
- He, J., Acharyya, K., & Vidalí, G. 2016, *ApJ*, **825**, 89
- He, J., Clements, A. R., Emtiaz, S., et al. 2019, *ApJ*, **878**, 94
- Henning, T., & Semenov, D. 2013, *Chem. Rev.*, **113**, 9016
- Keto, E., & Caselli, P. 2010, *MNRAS*, **402**, 1625
- Kimmel, G. A., Dohnálek, Z., Stevenson, K. P., Smith, R. S., & Kay, B. D. 2001a, *J. Chem. Phys.*, **114**, 5295
- Kimmel, G. A., Stevenson, K. P., Dohnálek, Z., Smith, R. S., & Kay, B. D. 2001b, *J. Chem. Phys.*, **114**, 5284
- Kruczkiewicz, F., Vitorino, J., Congiu, E., Theulé, P., & Dulieu, F. 2021, *A&A*, **652**, A29
- Martin-Doménech, R., Caro, G. M., Bueno, J., & Goesmann, F. 2014, *A&A*, **564**, A8
- Minissale, M., Aikawa, Y., Bergin, E., et al. 2022, *ACS Earth Space Chem.*, **6**, 597
- Noble, J., Theulé, P., Duvernay, F., et al. 2014, *Phys. Chem. Chem. Phys.*, **16**, 23604
- Öberg, K. I., Boogert, A. C. A., Pontoppidan, K. M., et al. 2011, *ApJ*, **740**, 109
- Pagani, L., Bacmann, A., Cabrit, S., & Vastel, C. 2007, *A&A*, **467**, 179
- Penteado, E., Walsh, C., & Cuppen, H. 2017, *ApJ*, **844**, 71
- Pineda, J. E., Harju, J., Caselli, P., et al. 2022, *AJ*, **163**, 294
- Poch, O., Istiqomah, I., Quirico, E., et al. 2020, *Science*, **367**, aaw7462
- Potapov, A., Theulé, P., Jäger, C., & Henning, T. 2019, *ApJ*, **878**, L20
- Qi, C., Öberg, K. I., Wilner, D. J., et al. 2013, *Science*, **341**, 630
- Redaelli, E., Bizzocchi, L., Caselli, P., et al. 2019, *A&A*, **629**, A15
- Sandqvist, A., Hjalmarsen, Å., Frisk, U., et al. 2017, *A&A*, **599**, A135
- Scott Smith, R., Zubkov, T., & Kay, B. D. 2006, *J. Chem. Phys.*, **124**, 114710
- Sipilä, O., Caselli, P., Redaelli, E., Juvela, M., & Bizzocchi, L. 2019, *MNRAS*, **487**, 1269
- Smith, R. S., Huang, C., Wong, E., & Kay, B. D. 1997, *Phys. Rev. Lett.*, **79**, 909
- Speedy, R. J., Debenedetti, P. G., Smith, R. S., Huang, C., & Kay, B. D. 1996, *J. Chem. Phys.*, **105**, 240
- Subasaria, T., Throuer, J., & Zacharias, H. 2015, *MNRAS*, **454**, 3317
- Tafalla, M., Myers, P., Caselli, P., Walmsley, C., & Comito, C. 2002, *ApJ*, **569**, 815
- Tafalla, M., Myers, P., Caselli, P., & Walmsley, C. 2004, *A&A*, **416**, 191
- Tinacci, L., Germain, A., Pantaleone, S., et al. 2022, *ACS Earth Space Chem.*, **6**, 1514
- Viti, S., Collings, M. P., Dever, J. W., McCoustra, M. R., & Williams, D. A. 2004, *MNRAS*, **354**, 1141

## Appendix A:

**Table A.1.** Additional experiments carried out to study the behaviour of ammonia with H<sub>2</sub>O, <sup>13</sup>CO, and CO<sub>2</sub> but not included in the main text.

No.	Experiment	Ratio	Quantity Deposited (ML)
1	{NH <sub>3</sub> + H <sub>2</sub> O}	1:3	5(NH <sub>3</sub> ), 16 (H <sub>2</sub> O)
2	{NH <sub>3</sub> + H <sub>2</sub> O}	1:1	5 of each
3	{NH <sub>3</sub> + CO <sub>2</sub> + <sup>13</sup> CO}	1:3:15	7.4 ( <sup>13</sup> CO), 1.7 (CO <sub>2</sub> ), 0.5 (NH <sub>3</sub> )
4	{NH <sub>3</sub> + CO <sub>2</sub> }	1:3	6 (NH <sub>3</sub> ), 18 (CO <sub>2</sub> )

for a site with a lower binding energy. Following this principle, at low dosages (< 1ML), peak desorption occurs at higher temperatures. As the dosage increases, this peak shifts to lower temperatures. Once every adsorption site on the substrate is occupied, the peak stops shifting to lower temperatures. At this stage, any other incoming NH<sub>3</sub> binds to another NH<sub>3</sub> already adsorbed on the surface, and the desorption then follows zeroth order kinetics. This can be seen as the increase in peak height (12 min curve and above in the figure) and the subsequent shifting of the curve towards higher temperatures. Our experiments obtained 1 ML for an exposure time higher than 8 minutes but lower than 12 minutes. Hence, we chose a time of 9 minutes, similar to the time we obtained for <sup>13</sup>CO and N<sub>2</sub> under similar beam conditions.

## Appendix B:

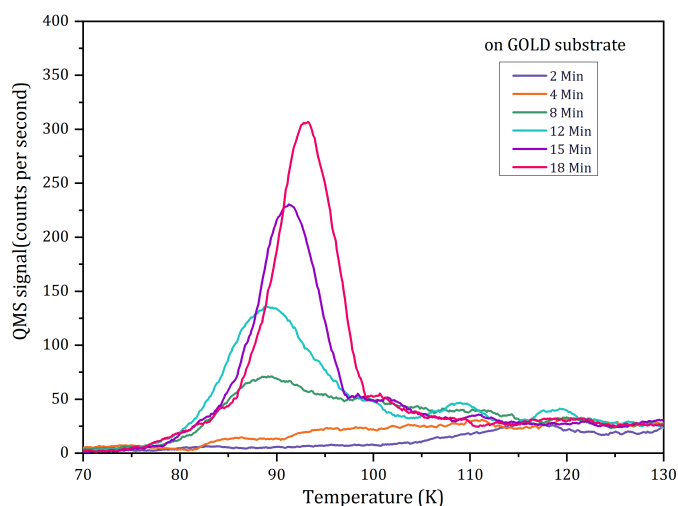


**Fig. B.1.** Experiments to calibrate for 1ML of NH<sub>3</sub>. TPD curves of NH<sub>3</sub> were deposited on a gold substrate for various dosages in order to calibrate for 1 ML. We used a constant flux of  $4.67 \times 10^{-5}$  mbar and varied the duration of injection to vary the dosage.

Figure B.1 shows the experiments performed to calibrate for 1 ML of NH<sub>3</sub>. Varying doses of NH<sub>3</sub> were deposited onto the gold substrate at 10K followed by a TPD. During deposition, adsorption sites with the highest binding energy were occupied first followed by sites of lower binding energy until all the sites on the substrate were occupied. Hence, a species adsorbed on a site with a higher binding energy desorbs at a higher temperature, as opposed to desorption at lower temperatures